Supporting Information

Functionalized nickel(II)-iron(II) dithiolates as biomimetic models of [NiFe]-H_2ases

Li-Cheng Song,* Yin-Peng Wang, Yi-Xiong Dong and Xi-Yue Yang

Contents:

1. IR and ^{1}H (^{13}C, ^{31}P) NMR spectra of [**1**]$(PF_6)_2$ (Fig. S1– Fig. S4)
2. In situ IR spectra showing the terminal CO changes of starting material [**C**]$(BF_4)_2$, intermediate $\mathbf{m_2}$ and product [**3**]BF_4 during reaction of [**C**]$(BF_4)_2$ with Me_3NO in pyridine (Fig. S5).
3. IR and ^{1}H (^{13}C, ^{31}P) NMR spectra of [**2**]PF_6 (Fig. S6– Fig. S9)
4. IR and ^{1}H (^{13}C, ^{31}P) NMR spectra of [**3**]BF_4 (Fig. S10–Fig. S13)
5. Bulk electrolysis for the two-electron reduction of $[CpFe(CO)_2]_2$ and the one-electron reduction of [**2**]PF_6 (Fig. S14)
6. Plots of i_p versus $v^{1/2}$ for the reduction peaks of [**2**]PF_6 (Fig. S15)
7. In situ IR spectra showing the terminal CO changes of starting material [**1**]$(PF_6)_2$, intermediate $\mathbf{m_3}$ and product [**4**]PF_6 during reaction of [**1**]$(PF_6)_2$ with Me_3NO and HCO_2H in acetone (Fig. S16)
8. In situ IR spectra showing the terminal CO changes of starting material [**1**]$(PF_6)_2$, intermediate $\mathbf{m_3}$ and product [**6**]PF_6 during reaction of [**1**]$(PF_6)_2$ with Me_3NO and $PhCO_2H$ in acetone (Fig. S17)
9. IR and ^{1}H (^{13}C, ^{31}P) NMR spectra of [**4**]PF_6 (Fig. S18– Fig. S21)
10. IR and ^{1}H (^{13}C, ^{31}P) NMR spectra of [**5**]PF_6 (Fig. S22– Fig. S25)
11. IR and ^{1}H (^{13}C, ^{31}P) NMR spectra of [**6**]PF_6 (Fig. S26– Fig. S29)
12. IR and ^{1}H (^{13}C, ^{31}P) NMR spectra of [**7**]PF_6 (Fig. S30– Fig. S33)
13. IR and ^{1}H (^{13}C, ^{31}P) NMR spectra of [**8**]PF_6 (Fig. S34– Fig. S37)
14. IR and ^{1}H (^{13}C, ^{31}P) NMR spectra of [**9**]$(PF_6)_2$ (Fig. S38– Fig. S41)
15. IR and ^{1}H (^{13}C, ^{31}P) NMR spectra of [**9**]$(BF_4)_2$ (Fig. S42– Fig. S45)
16. References

1. IR and ^{1}H (^{13}C, ^{31}P) NMR spectra of [**1**]$(PF_6)_2$

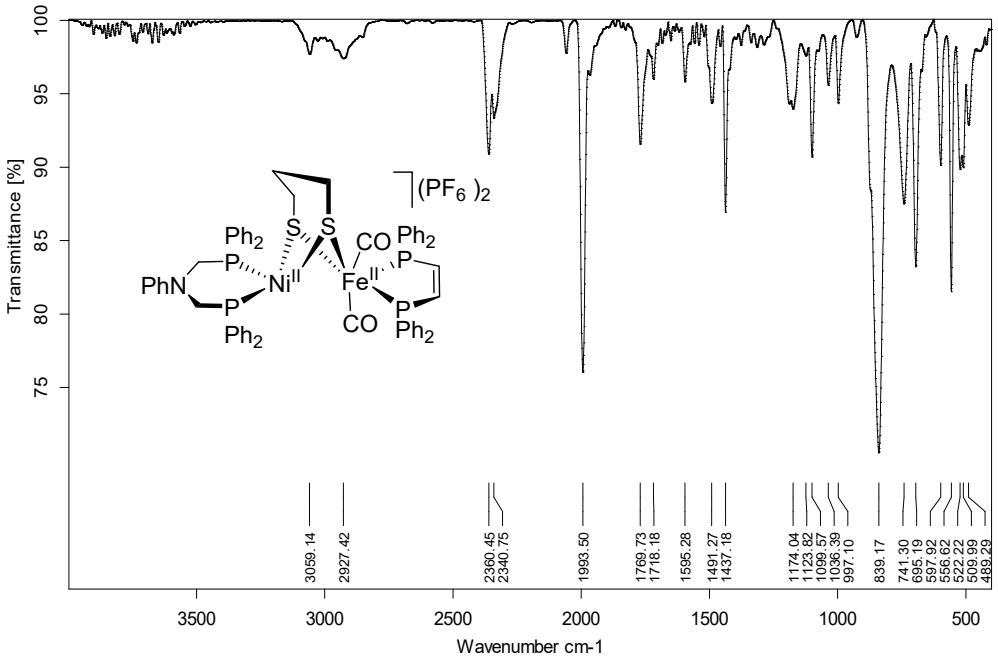

Fig. S1 IR spectrum of [**1**]$(PF_6)_2$

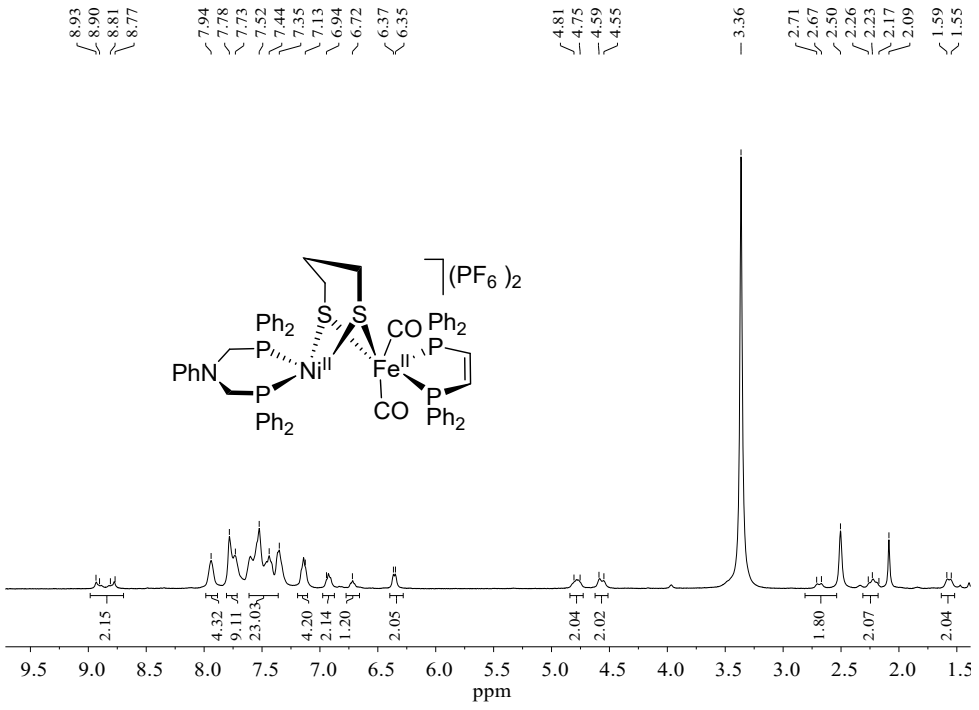

Fig. S2 ^{1}H NMR spectrum of [**1**]$(PF_6)_2$

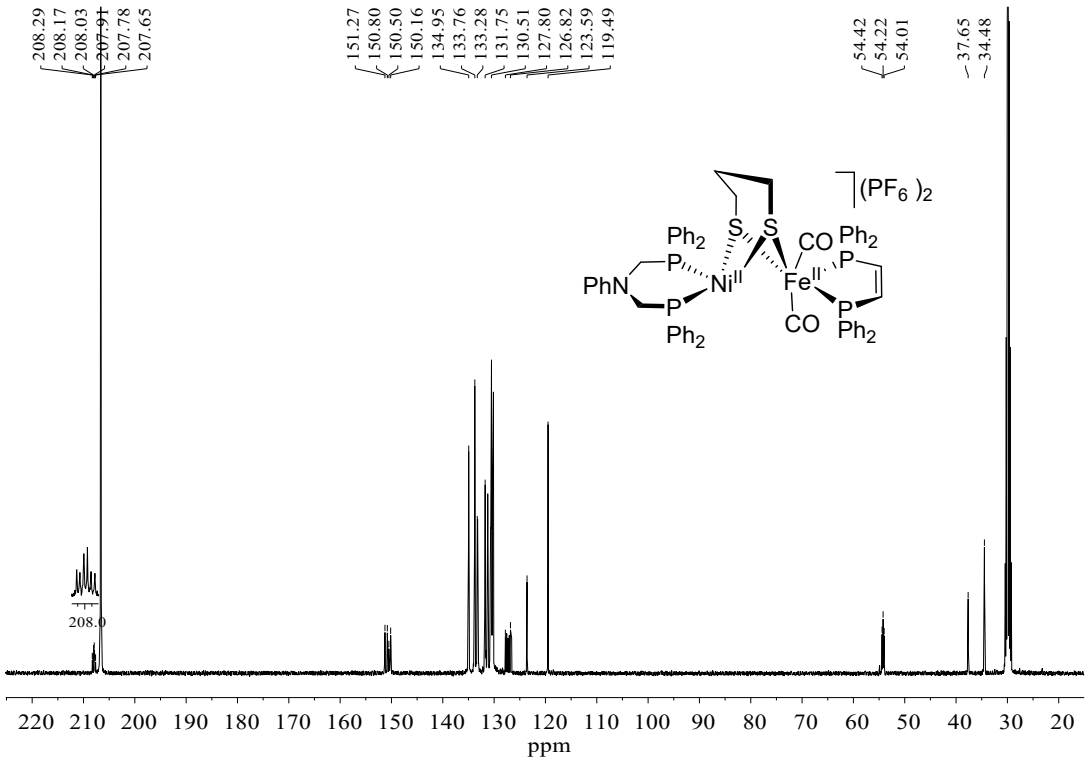

Fig. S3 ^{13}C NMR spectrum of [**1**]$(PF_6)_2$

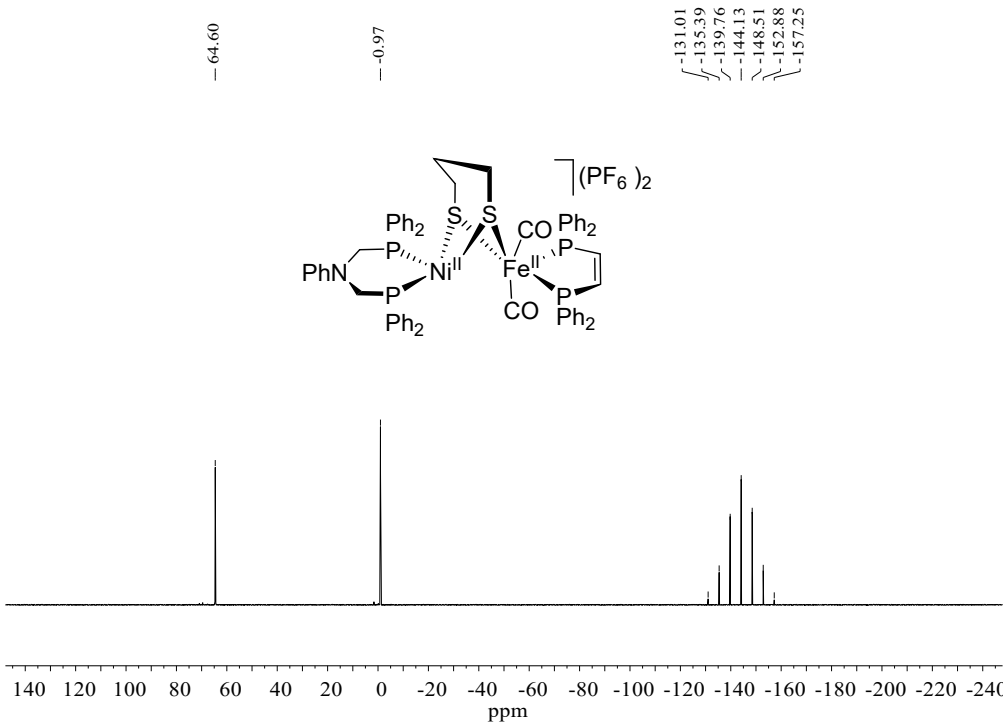

Fig. S4 ^{31}P NMR spectrum of [**1**]$(PF_6)_2$

2. In situ IR spectra showing the terminal CO changes of starting material [**C**]$(BF_4)_2$, intermediate $\mathbf{m_2}$ and product [**3**]BF_4 during reaction of [**C**]$(BF_4)_2$ with Me_3NO in pyridine.

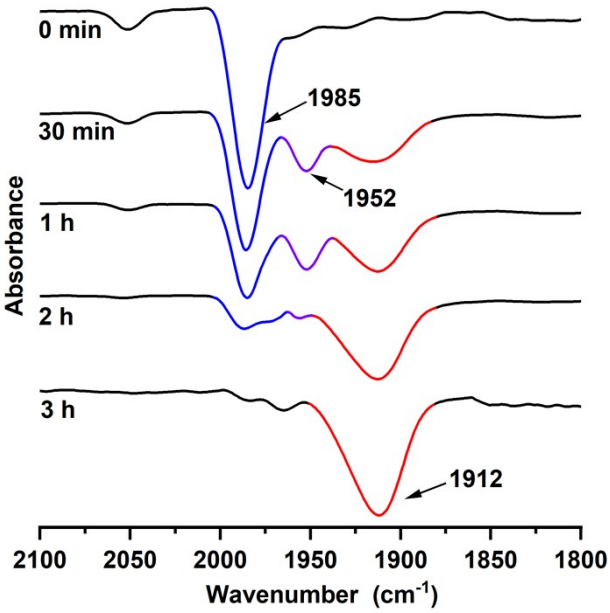

Fig. S5 In situ IR spectra showing the terminal CO changes of starting material [**C**]$(BF_4)_2$, intermediate $\mathbf{m_2}$ and product [**3**]BF_4 during reaction of [**C**]$(BF_4)_2$ with Me_3NO in pyridine.

3. IR and ^{1}H (^{13}C, ^{31}P) NMR spectra of [**2**]PF_6

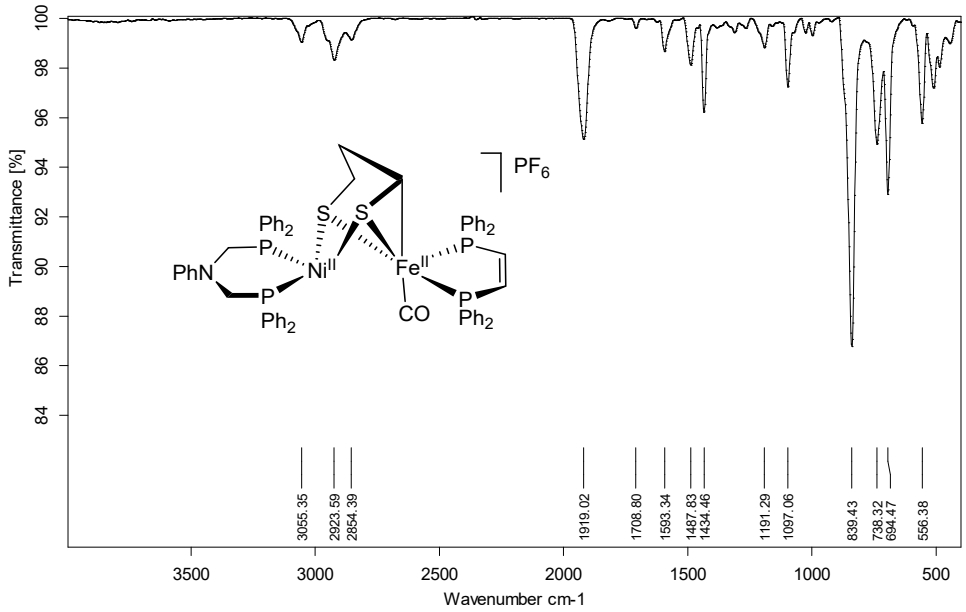

Fig. S6 IR spectrum of [**2**]PF_6

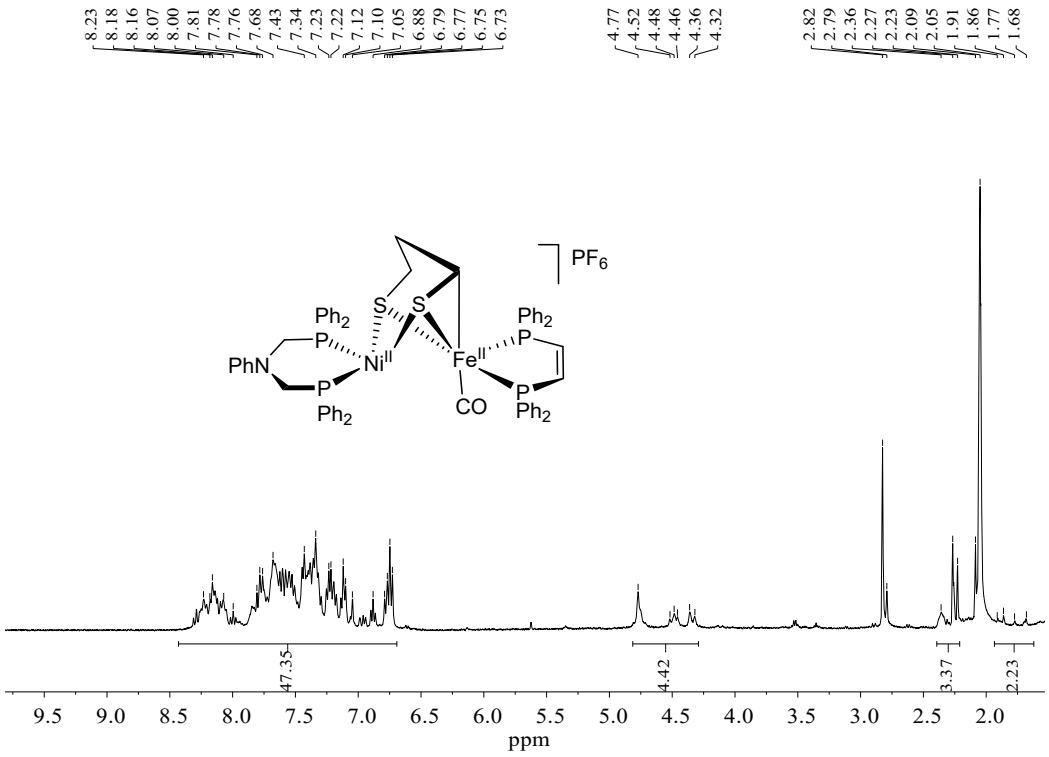

Fig. S7 ^{1}H NMR spectrum of [**2**]PF_6

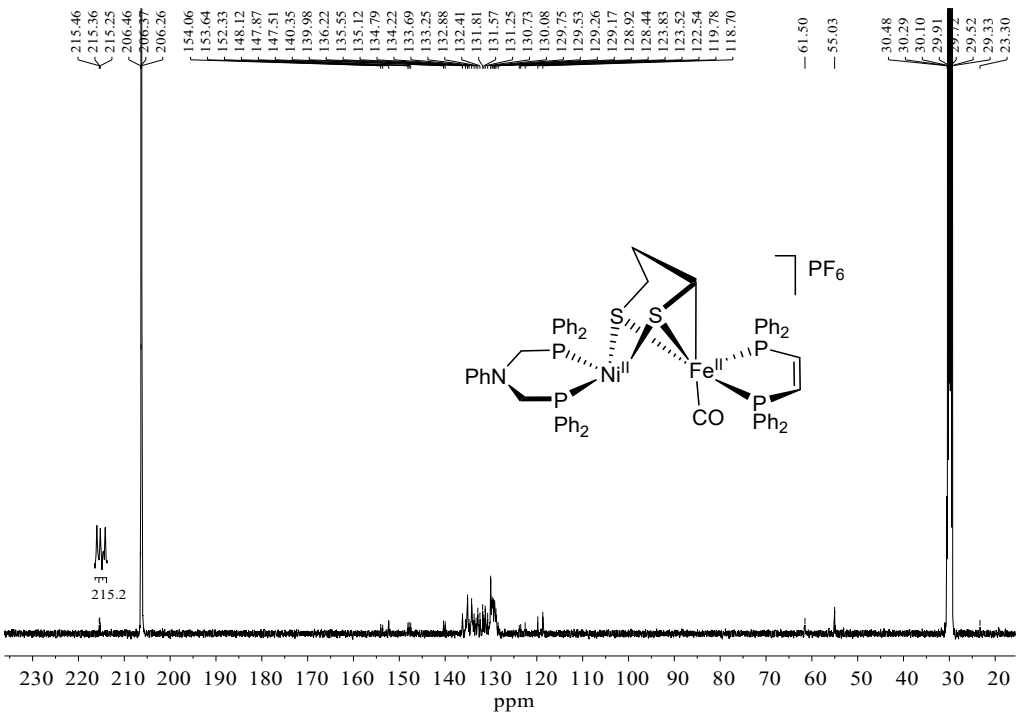

Fig. S8 ^{13}C NMR spectrum of [**2**]PF_6

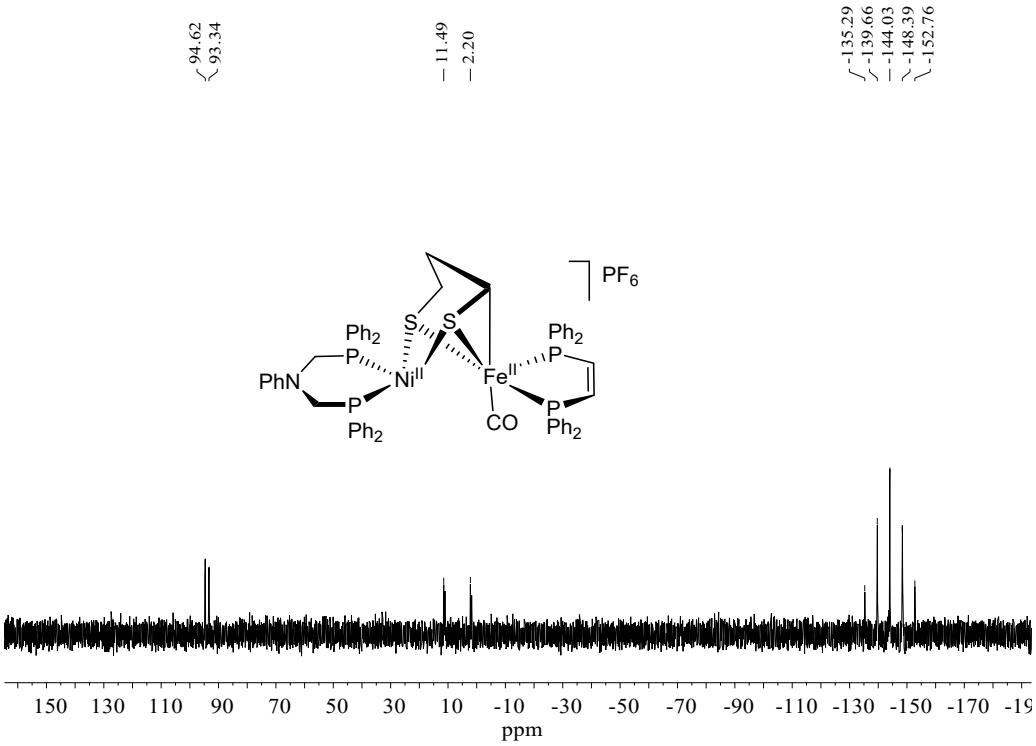

Fig. S9 ^{31}P NMR spectrum of [**2**]PF_6

4. IR and ^{1}H (^{13}C, ^{31}P) NMR spectra of [**3**]BF_4

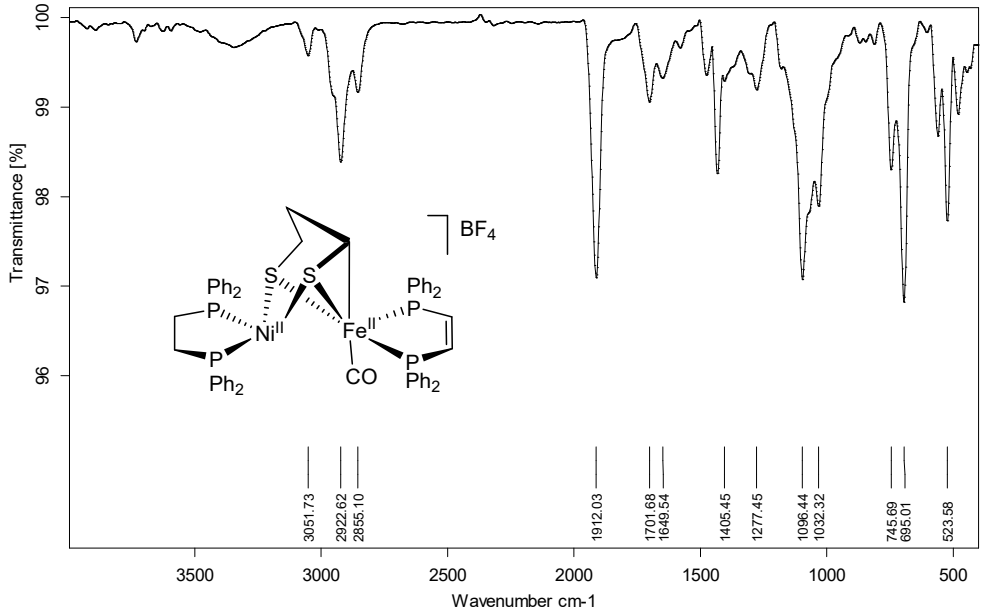

Fig. S10 IR spectrum of [**3**]BF_4

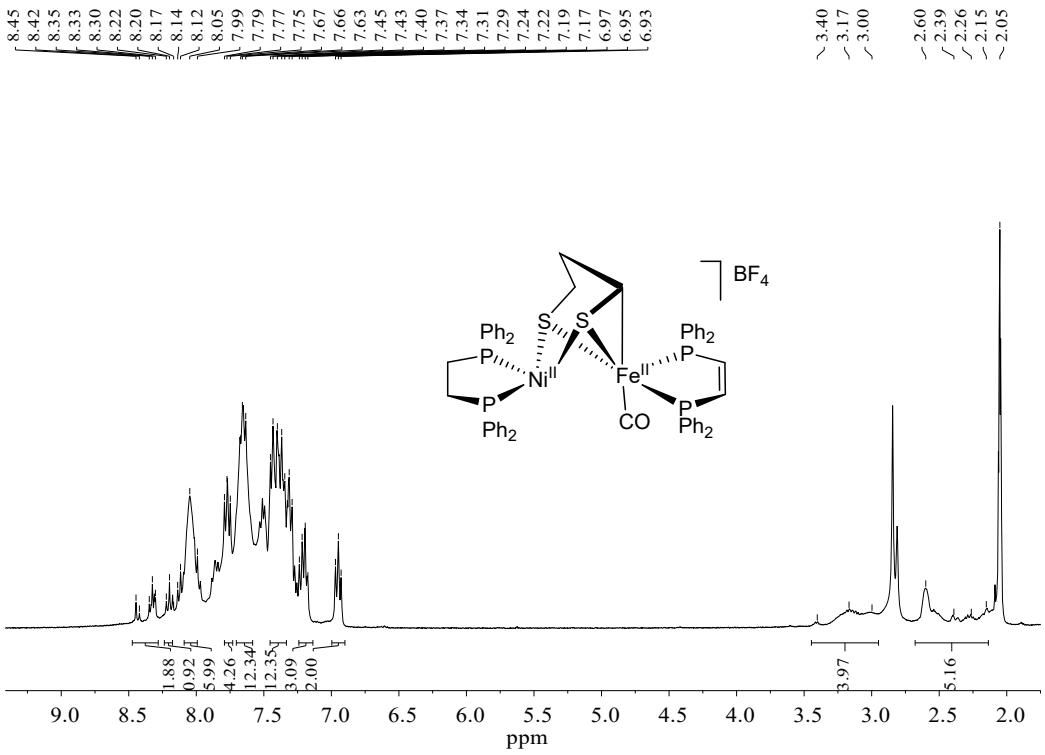

Fig. S11 ^{1}H NMR spectrum of [**3**]BF_4

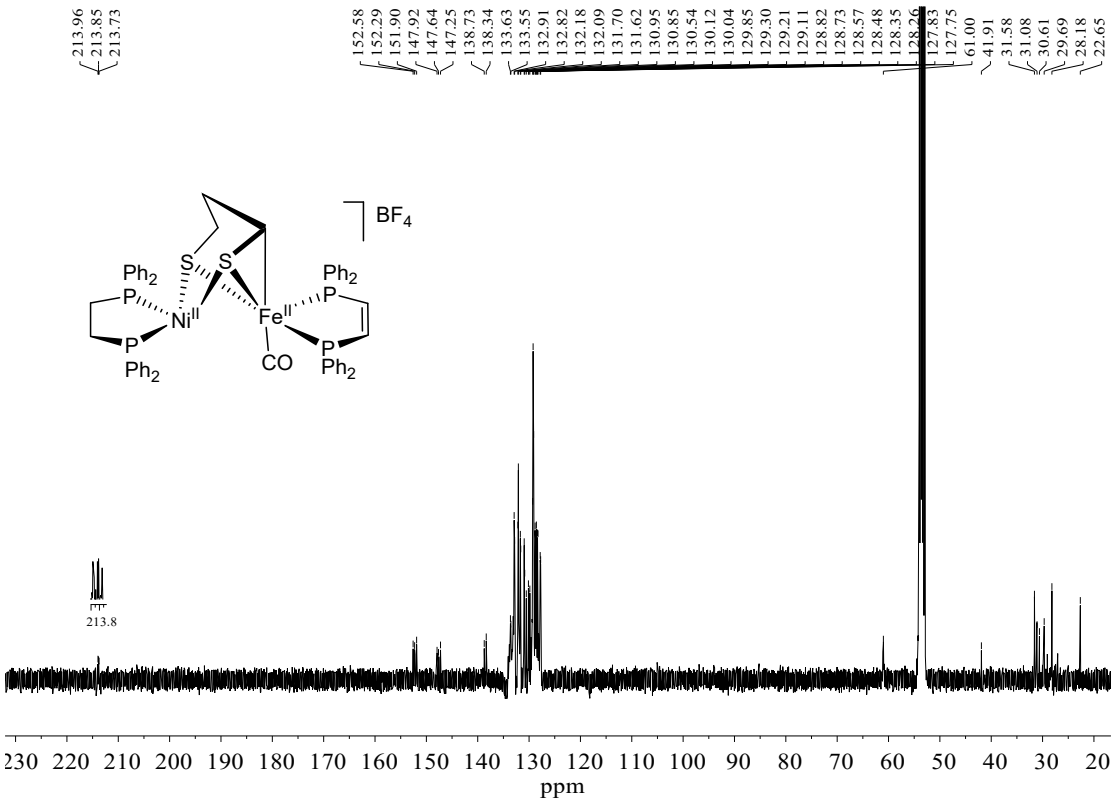

Fig. S12 ^{13}C NMR spectrum of [**3**]BF_4

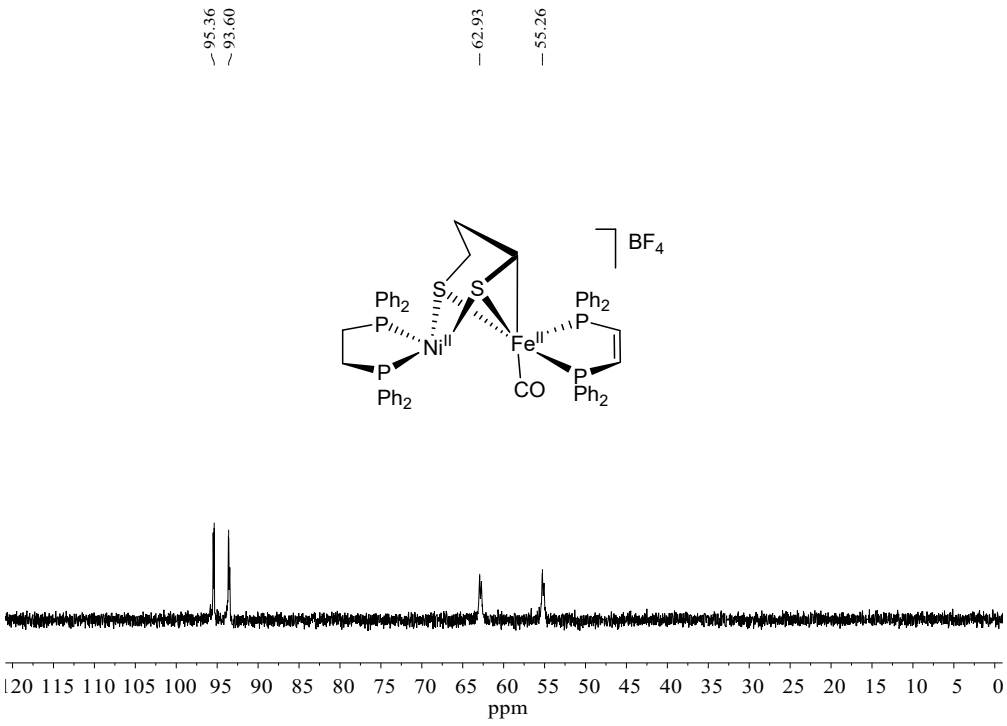

Fig. S13 ^{31}P NMR spectrum of [**3**]BF_4

5. Bulk electrolysis for the two-electron reduction of $[CpFe(CO)_2]_2$ and the one-electron reduction of [**2**]PF_6

The reduction event for [**2**]PF_6 is a one-electron process since their final Q values determined by bulk electrolysis are close to half that of the known two-electron reduction process of dimer $[CpFe(CO)_2]_2$.[1,2]

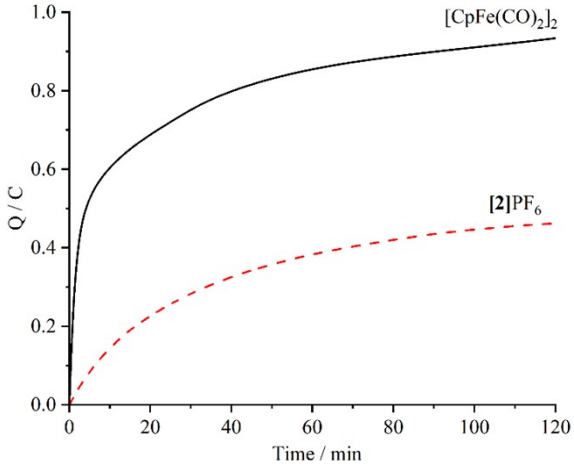

Fig. S14 Bulk electrolysis for the two-electron reduction of $[CpFe(CO)_2]_2$ and the one-electron reductions for the first reduction event of [**2**]PF_6.

6. Plots of i_p versus $v^{1/2}$ for the reduction peaks of [**2**]PF_6

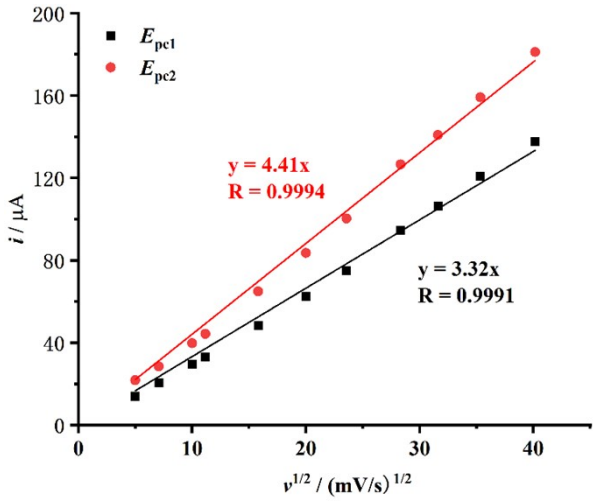

Fig. S15 Plots of i_p versus $v^{1/2}$ for the first and second reduction peaks of **[2]**PF_6 with their correlation coefficient R values.

7. In situ IR spectra showing the terminal CO changes of starting material [**1**]$(PF_6)_2$, intermediate $\mathbf{m_3}$ and product [**4**]PF_6 during reaction of [**1**]$(PF_6)_2$ with Me_3NO and HCO_2H in acetone.

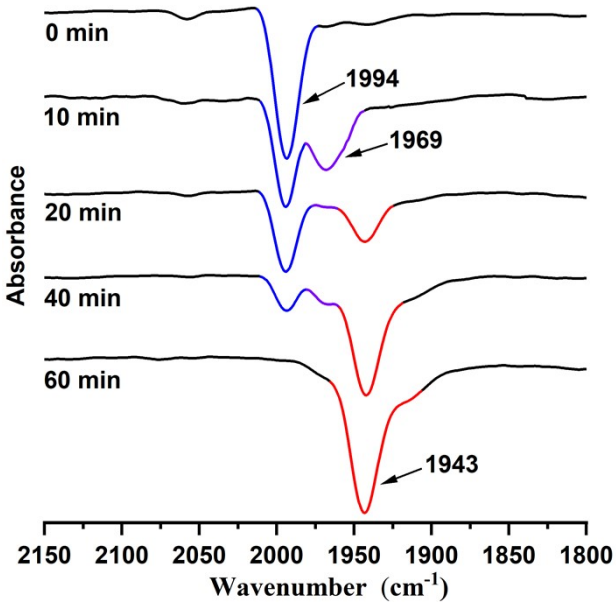

Fig. S16 In situ IR spectra showing the terminal CO changes of starting material [**1**]$(PF_6)_2$, intermediate $\mathbf{m_3}$ and product [**4**]PF_6 during reaction of [**1**]$(PF_6)_2$ with Me_3NO and HCO_2H in acetone.

8. In situ IR spectra showing the terminal CO changes of starting material [**1**]$(PF_6)_2$, intermediate $\mathbf{m_3}$ and product [**6**]PF_6 during reaction of [**1**]$(PF_6)_2$ with Me_3NO and $PhCO_2H$ in acetone.

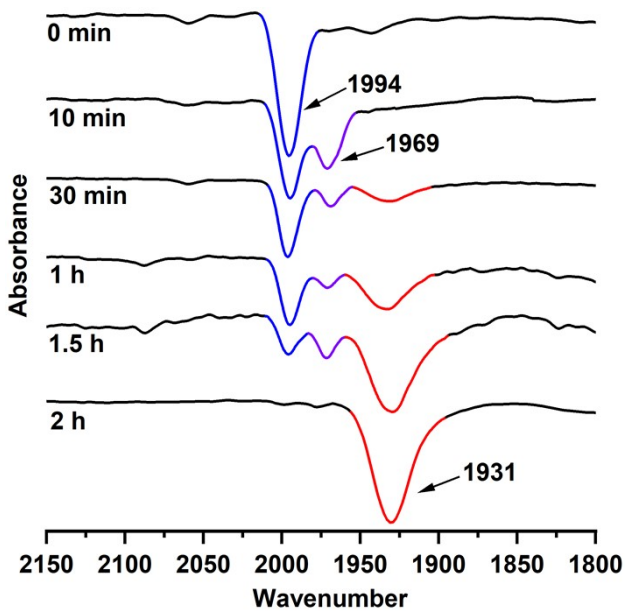

Fig. S17 In situ IR spectra showing the terminal CO changes of starting material [**1**]$(PF_6)_2$, intermediate $\mathbf{m_3}$ and product [**6**]PF_6 during reaction of [**1**]$(PF_6)_2$ with Me_3NO and $PhCO_2H$ in acetone.

9. IR and ^{1}H (^{13}C, ^{31}P) NMR spectra of [**4**]PF_6

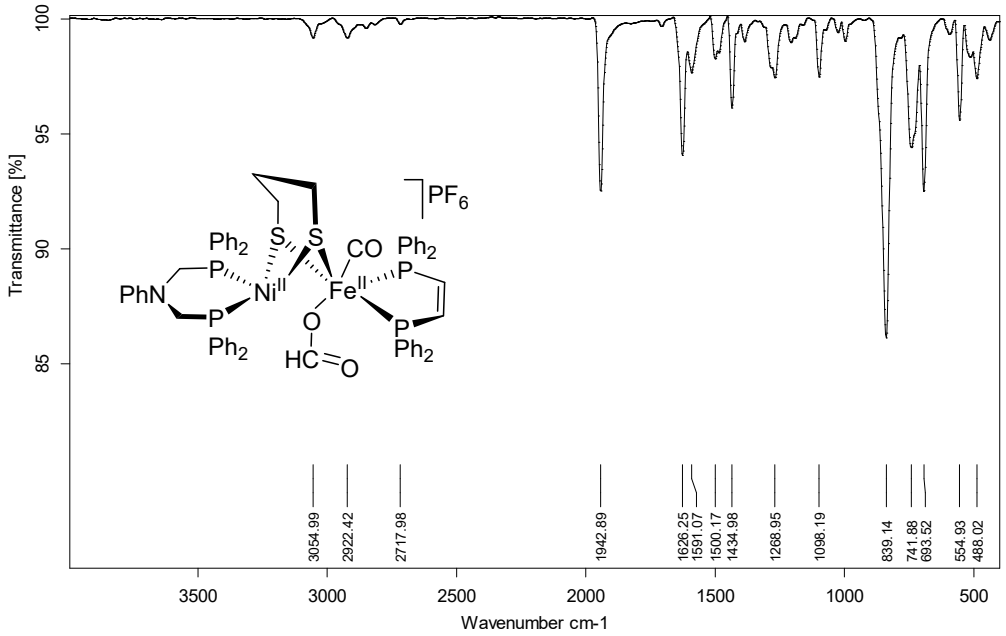

Fig. S18 IR spectrum of [**4**]PF_6

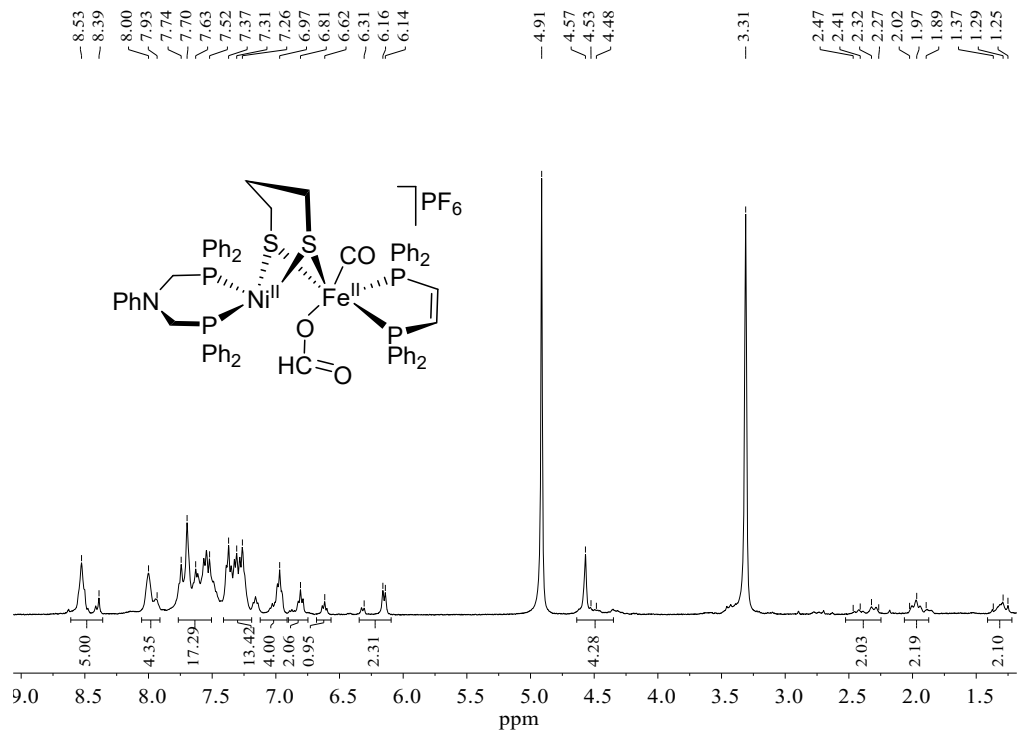

Fig. S19 ^{1}H NMR spectrum of [**4**]PF_6

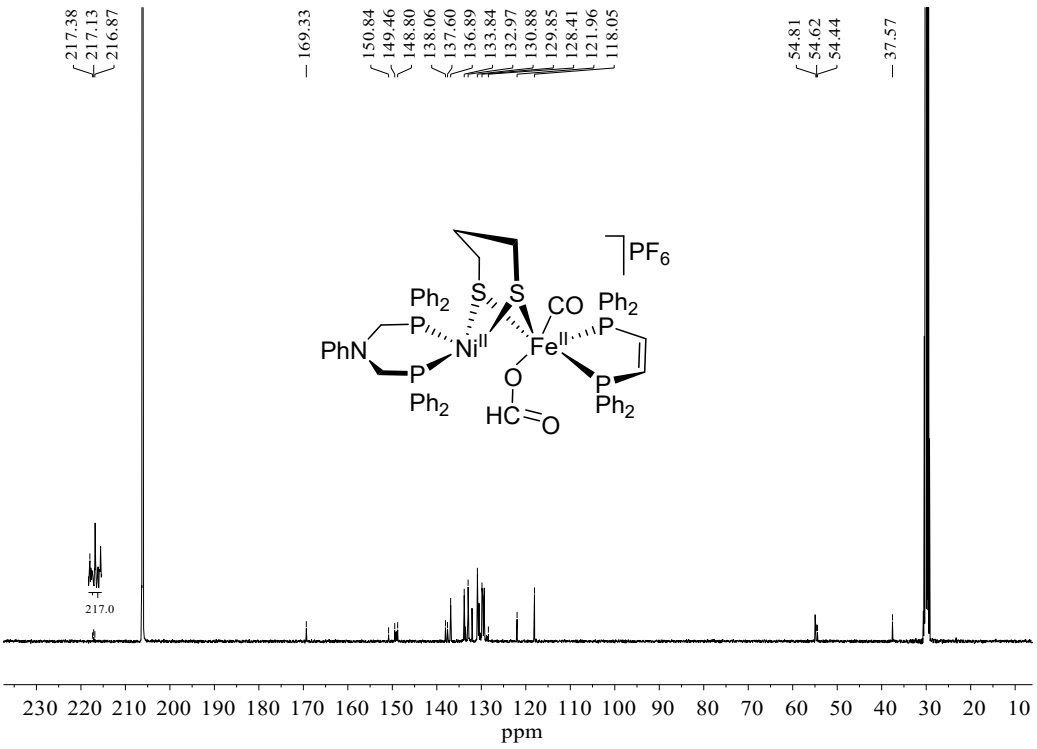

Fig. S20 ^{13}C NMR spectrum of [**4**]PF_6

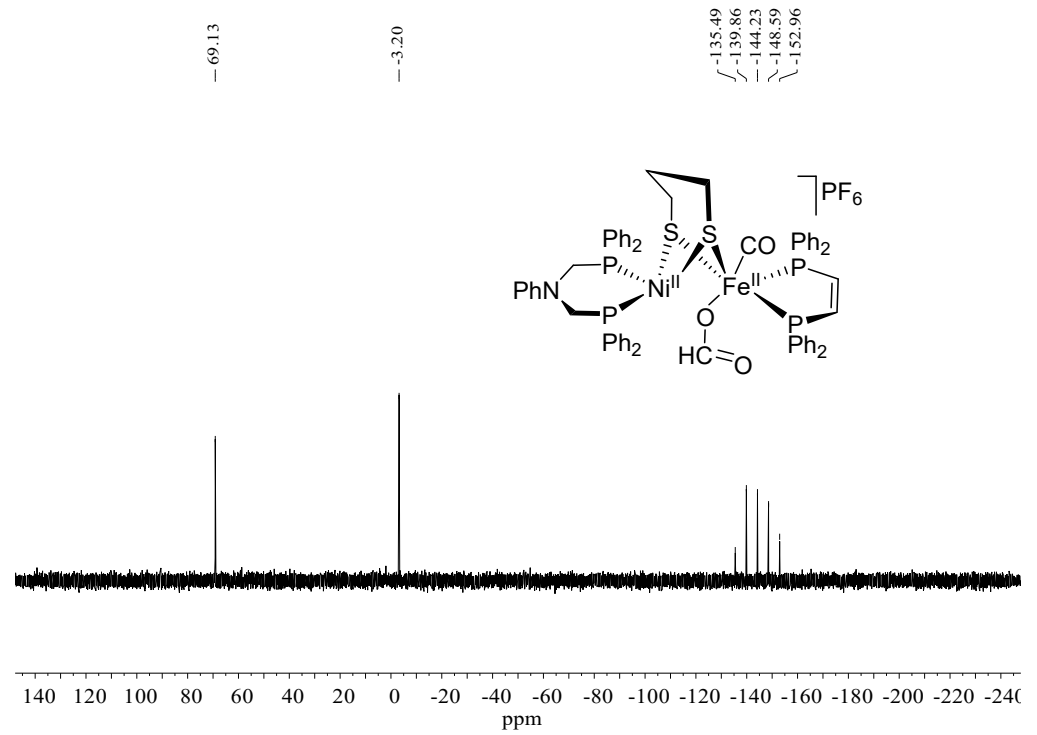

Fig. S21 ^{31}P NMR spectrum of [**4**]PF_6

10. IR and ^{1}H (^{13}C, ^{31}P) NMR spectra of [**5**]PF_6

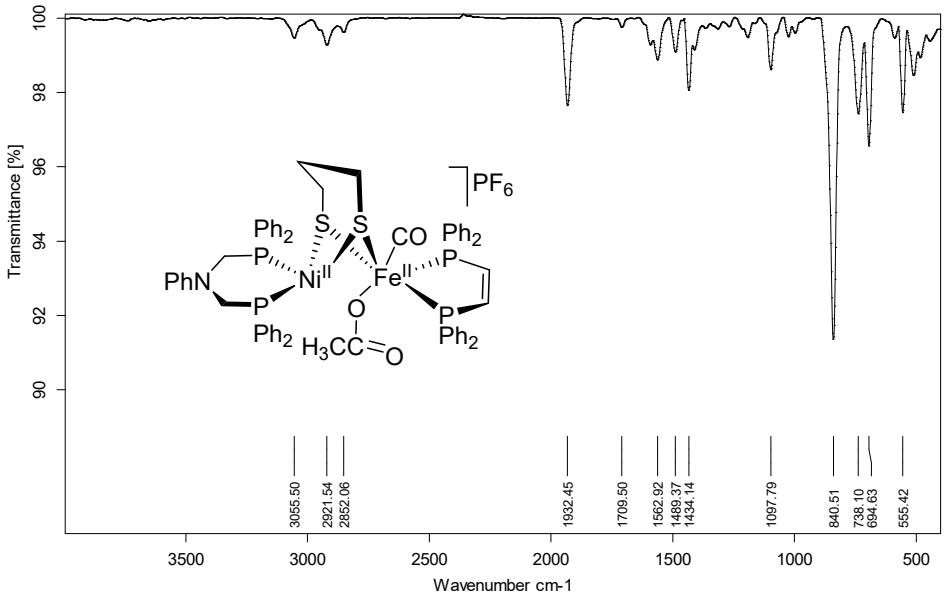

Fig. S22 IR spectrum of [**5**]PF_6

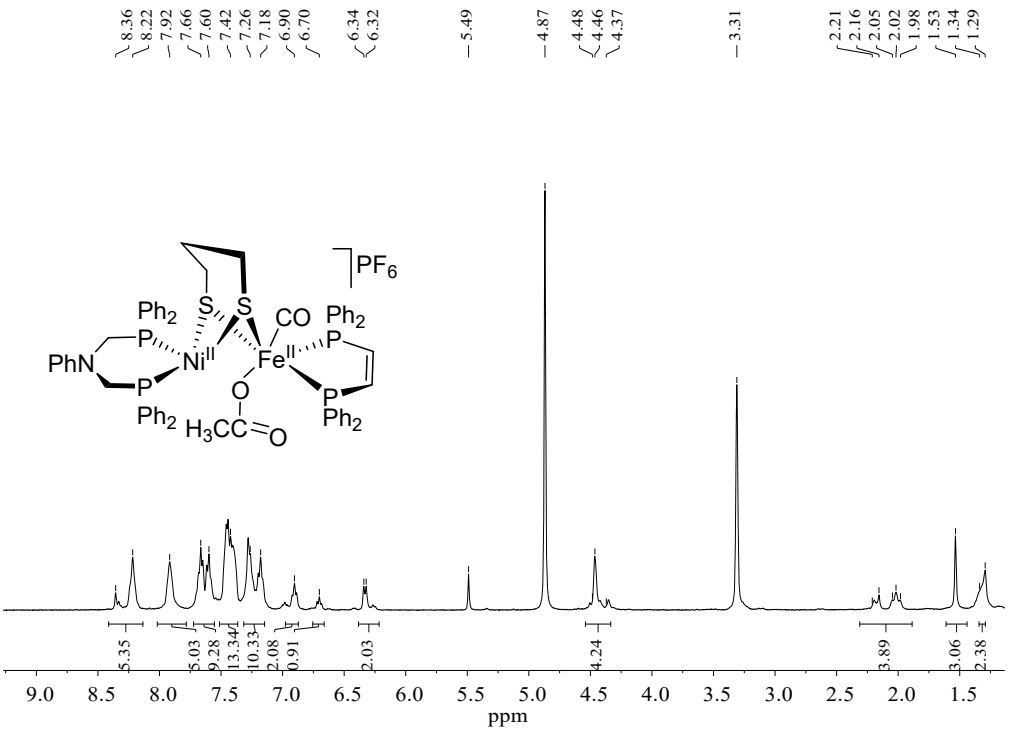

Fig. S23 ^{1}H NMR spectrum of [**5**]PF_6

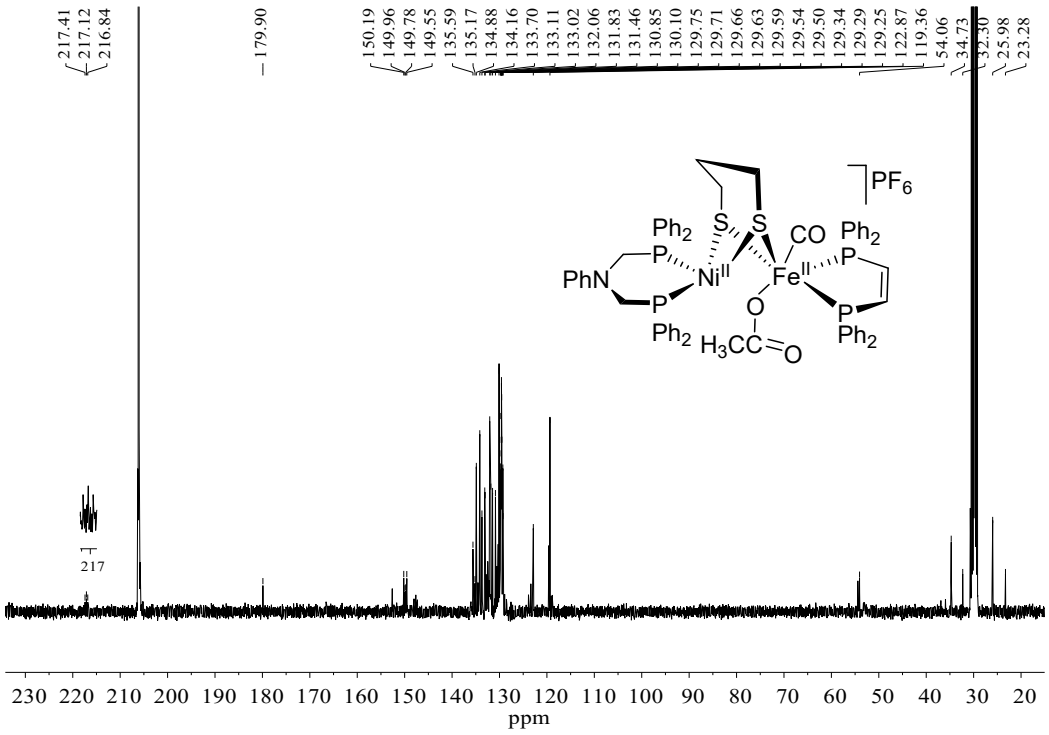

Fig. S24 ^{13}C NMR spectrum of [**5**]PF_6

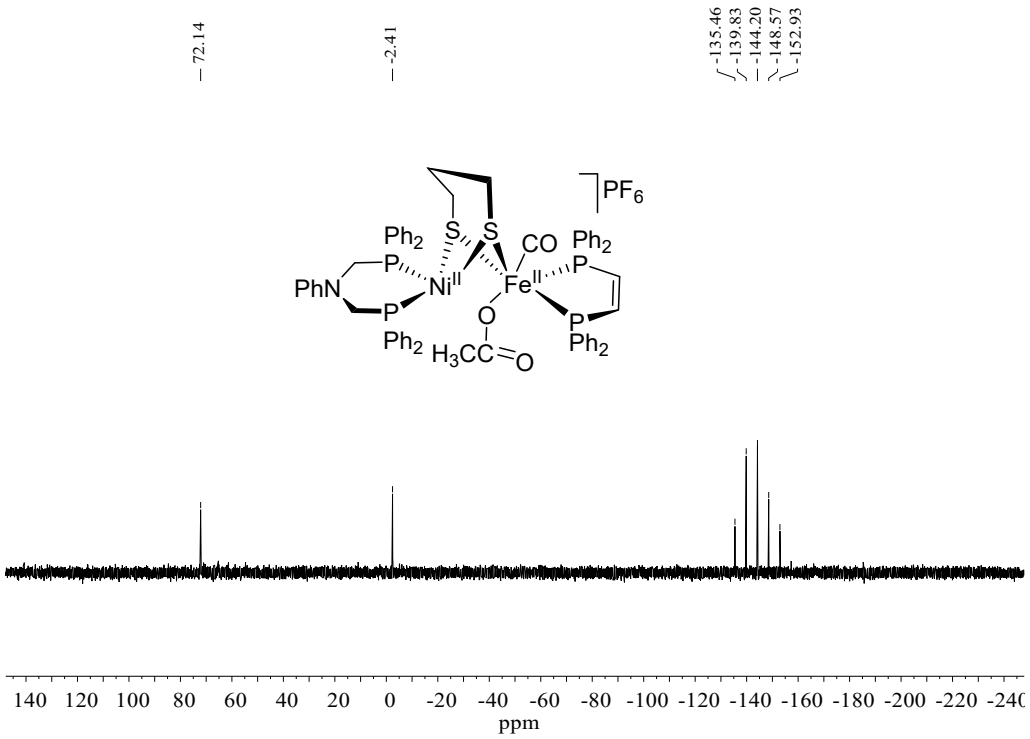

Fig. S25 ^{31}P NMR spectrum of [**5**]PF_6

11. IR and ^{1}H (^{13}C, ^{31}P) NMR spectra of [**6**]PF_6

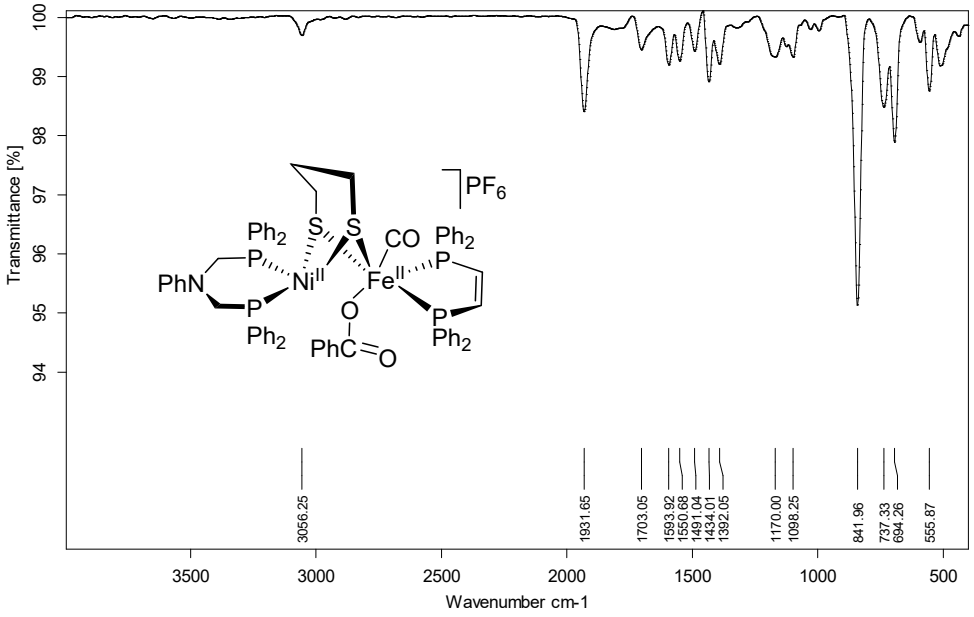

Fig. S26 IR spectrum of [**6**]PF_6

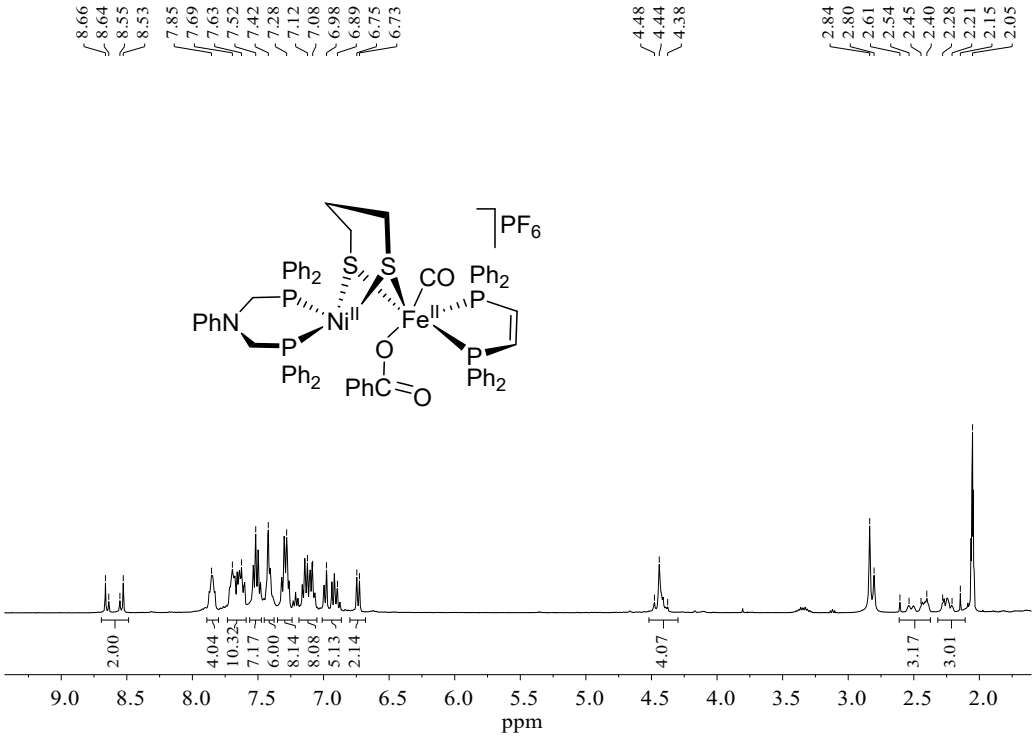

Fig. S27 ^{1}H NMR spectrum of [**6**]PF_6

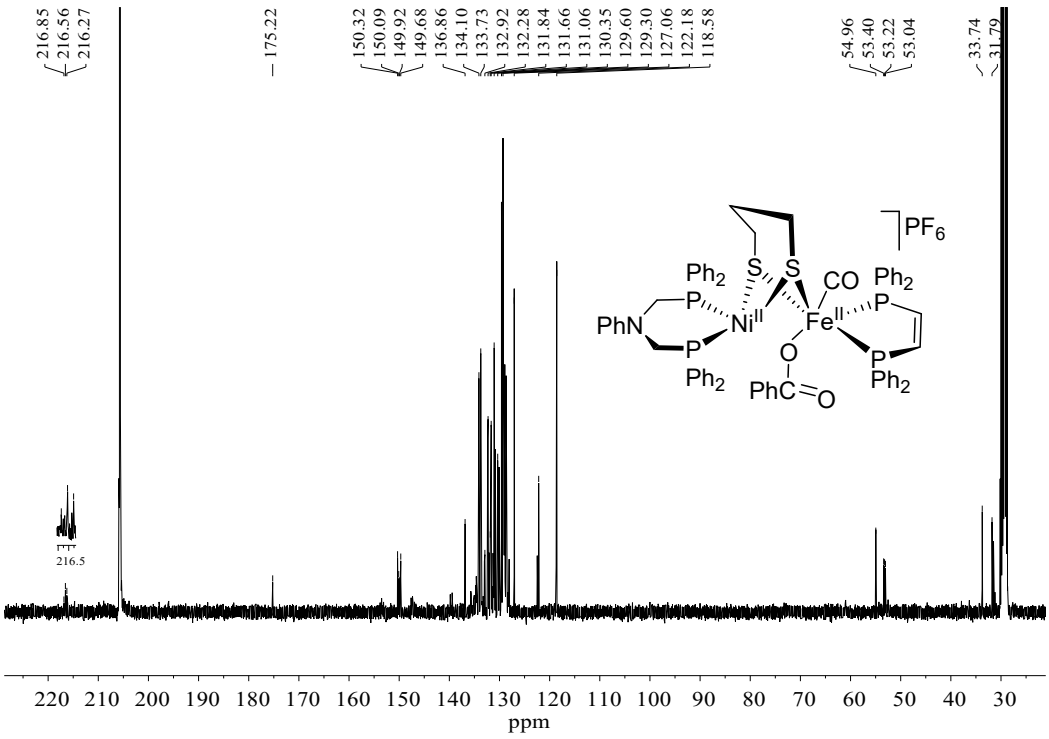

Fig. S28 ^{13}C NMR spectrum of [**6**]PF_6

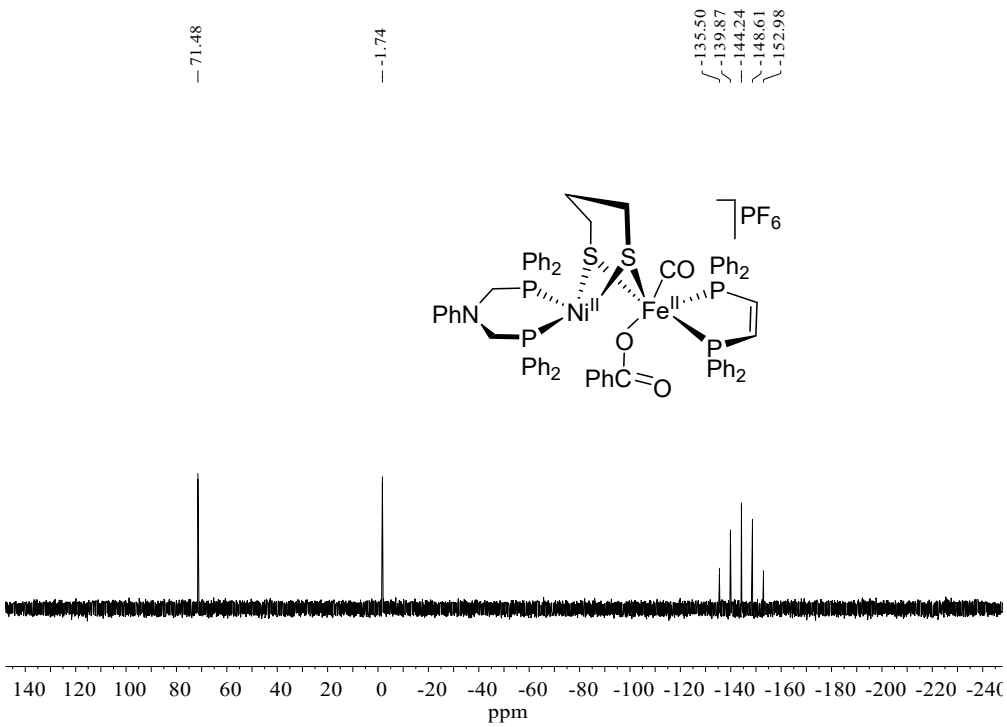

Fig. S29 ^{31}P NMR spectrum of [**6**]PF_6

12. IR and ^{1}H (^{13}C, ^{31}P) NMR spectra of [**7**]PF_6

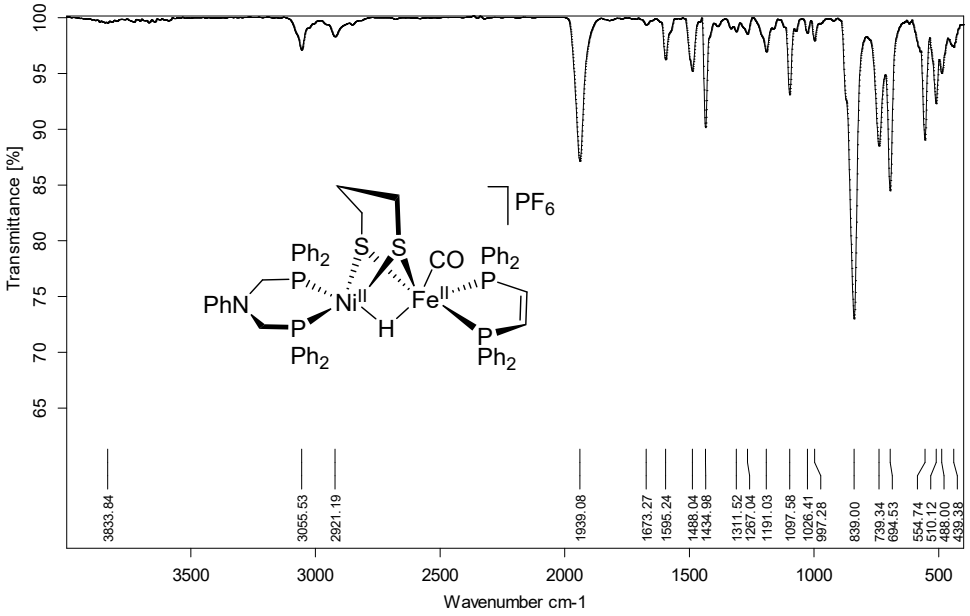

Fig. S30 IR spectrum of [**7**]PF_6

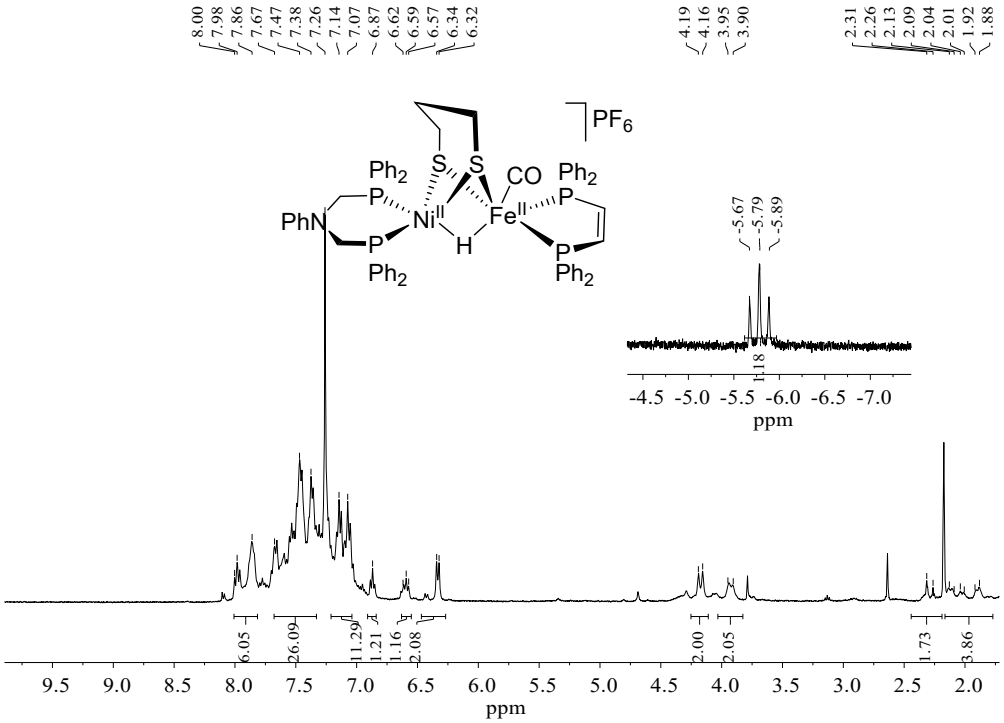

Fig. S31 ^{1}H NMR spectrum of [**7**]PF_6

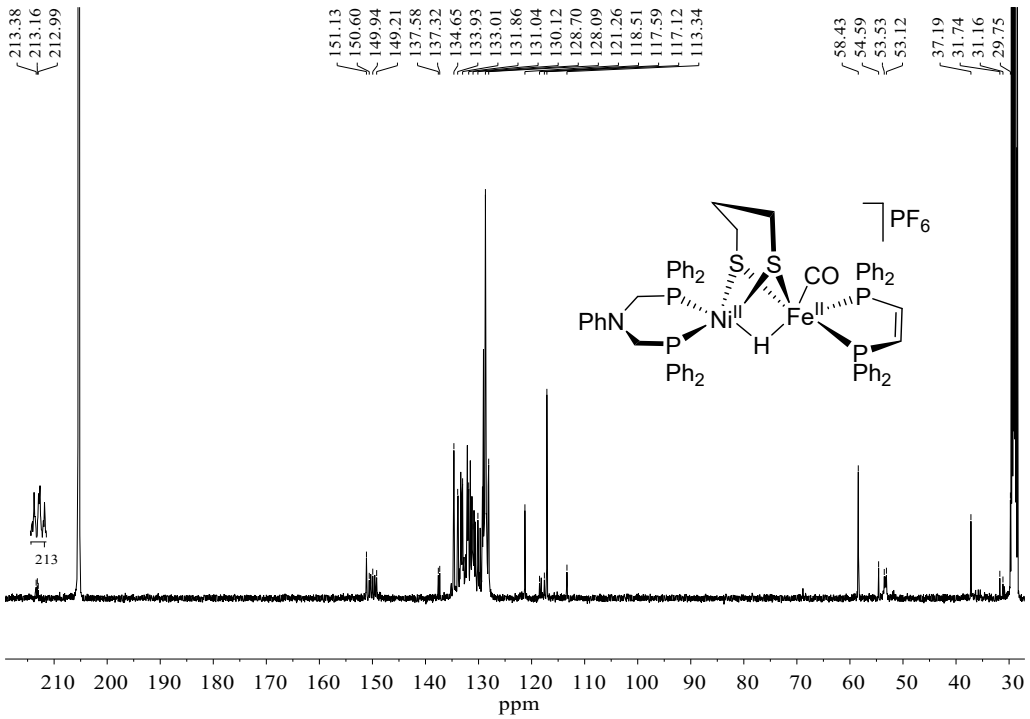

Fig. S32 ^{13}C NMR spectrum of [**7**]PF_6

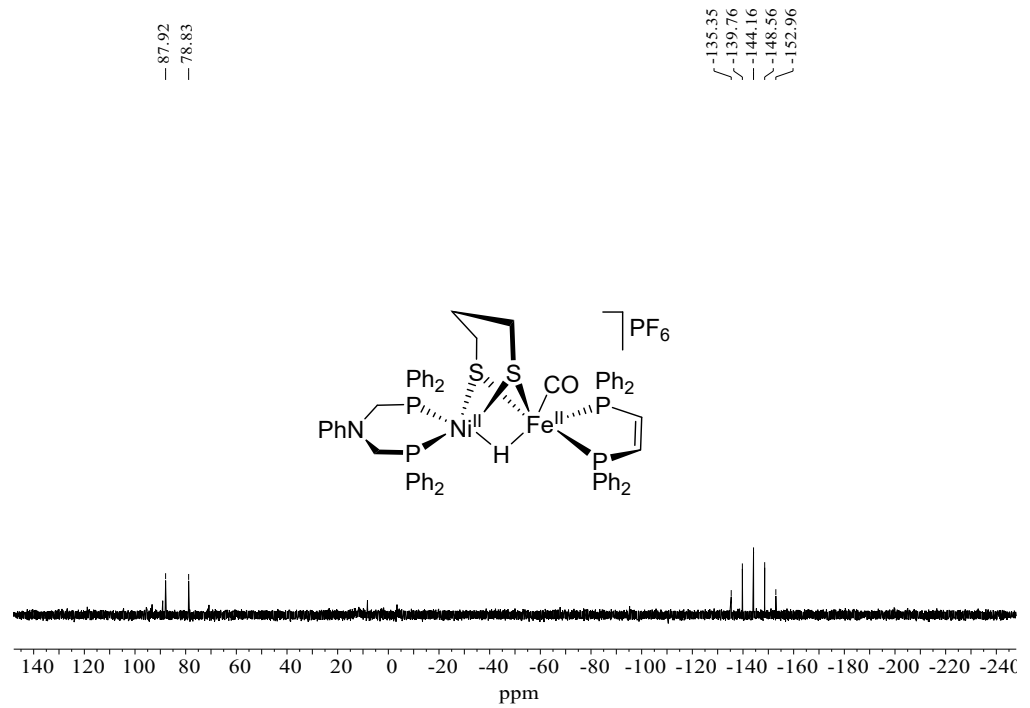

Fig. S33 ^{31}P NMR spectrum of [**7**]PF_6

13. IR and ^{1}H (^{13}C, ^{31}P) NMR spectra of [**8**]PF_6

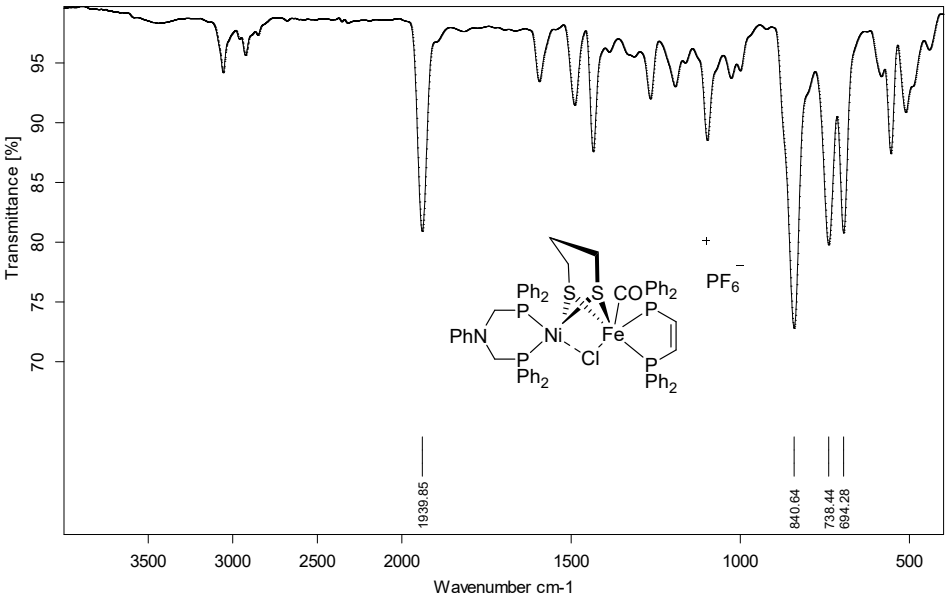

Fig. S34 IR spectrum of [**8**]PF_6

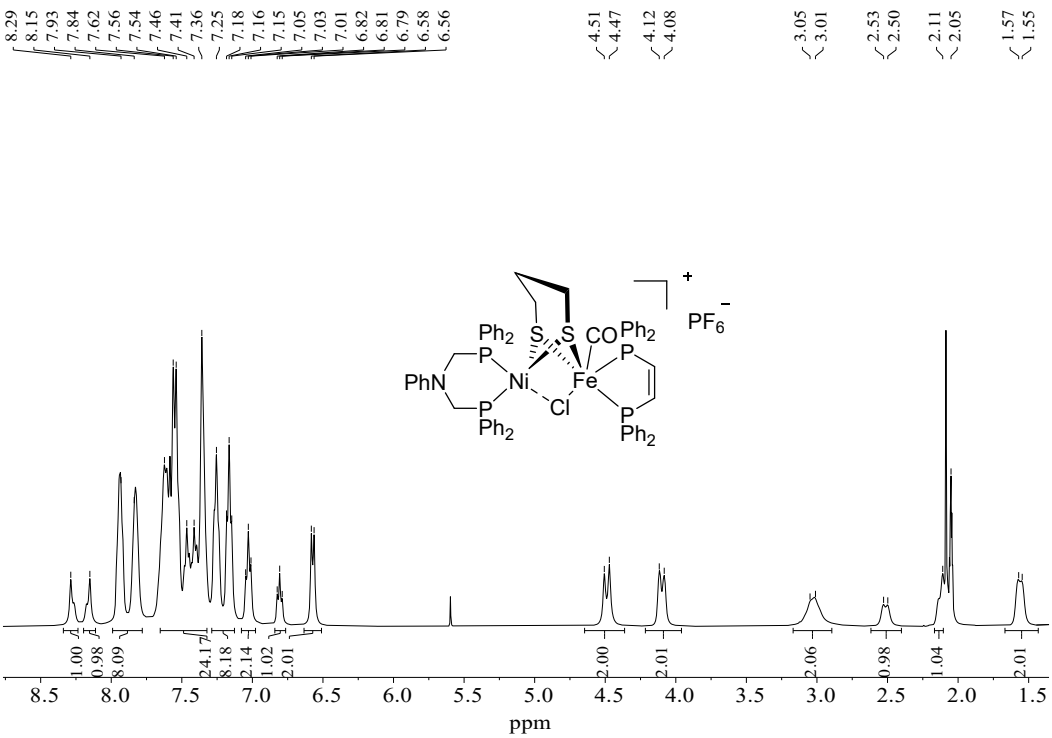

Fig. S35 ^{1}H NMR spectrum of [**8**]PF_6

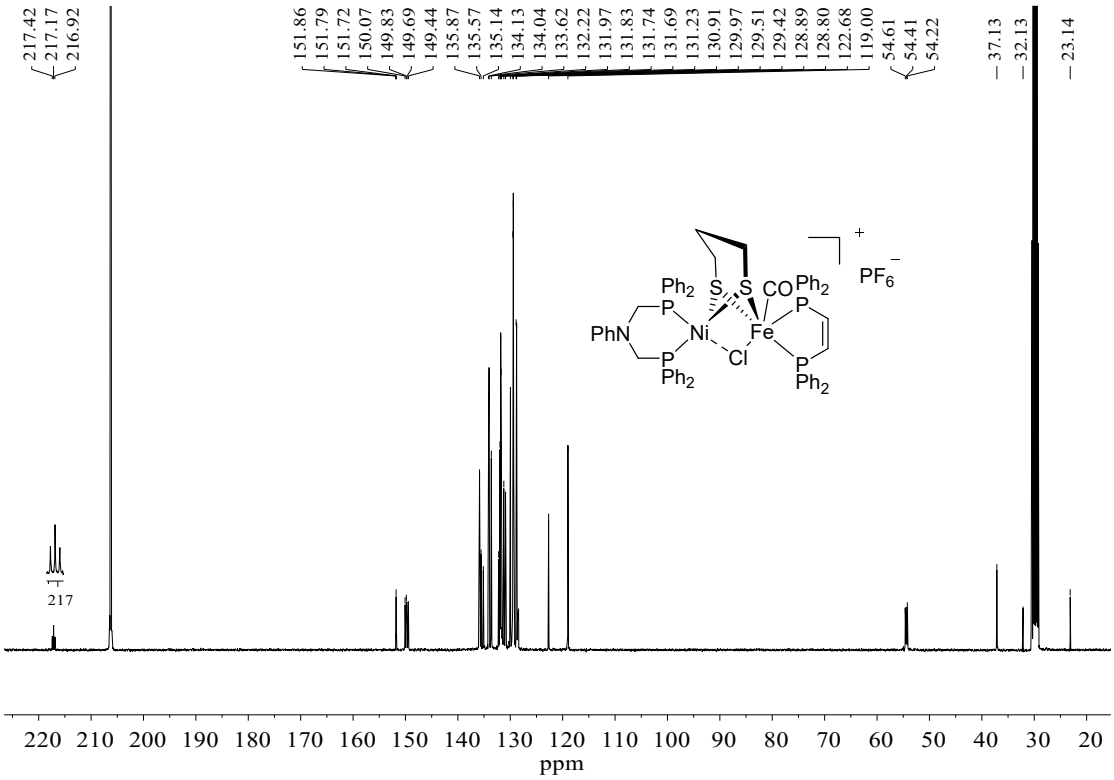

Fig. S36 ^{13}C NMR spectrum of [**8**]PF_6

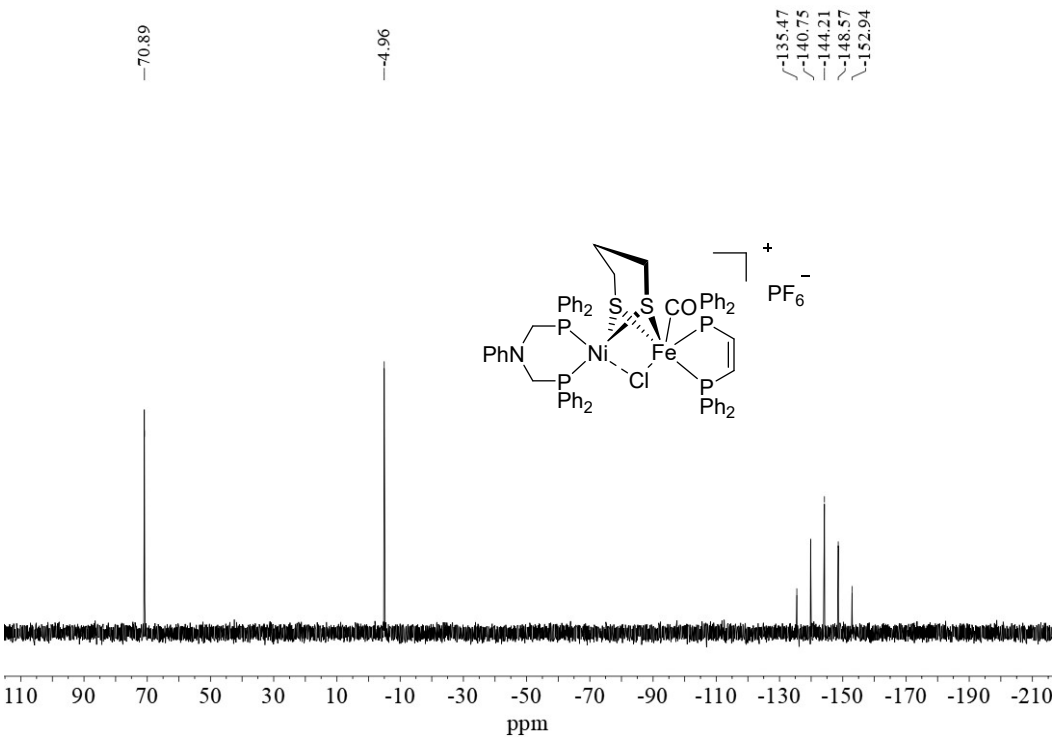

Fig. S37 ^{31}P NMR spectrum of [**8**]PF_6

14. IR and ^{1}H (^{13}C, ^{31}P) NMR spectra of [**9**]$(PF_6)_2$

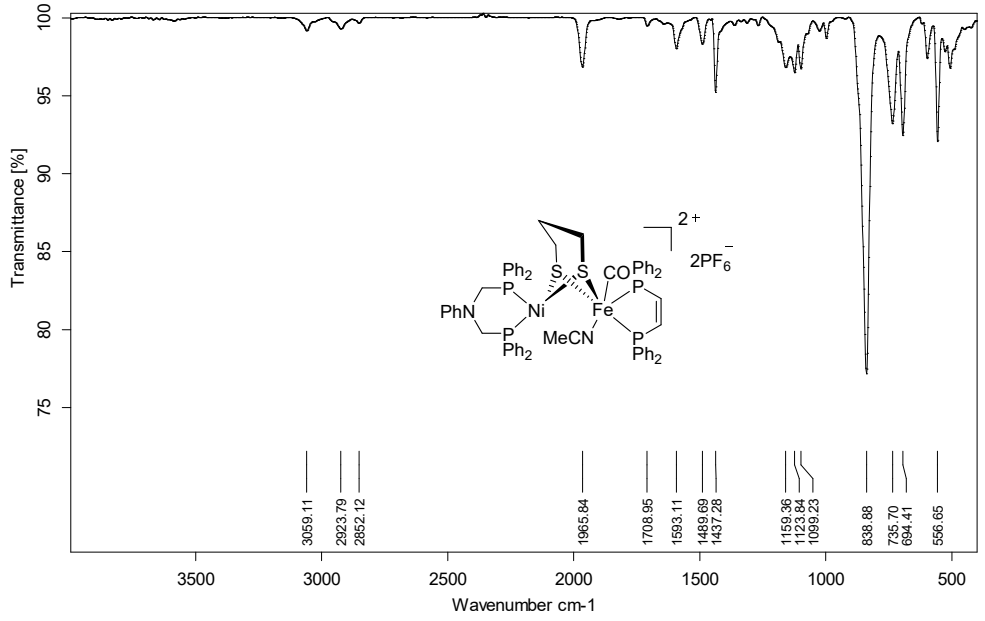

Fig. S38 IR spectrum of [**9**]$(PF_6)_2$

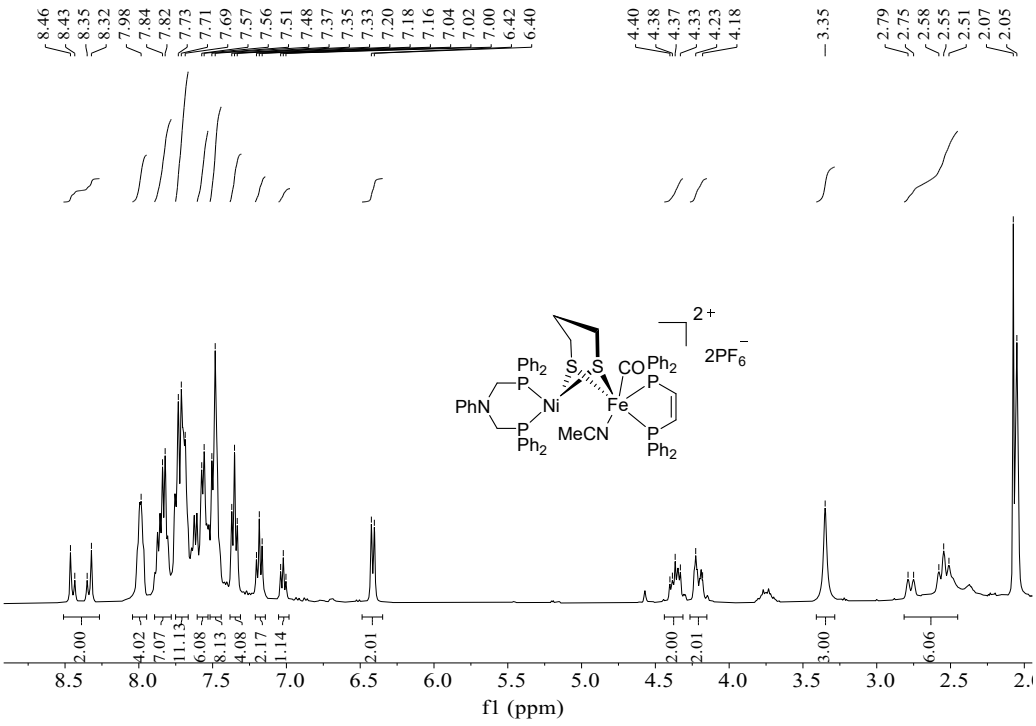

Fig. S39 ^{1}H NMR spectrum of [**9**]$(PF_6)_2$

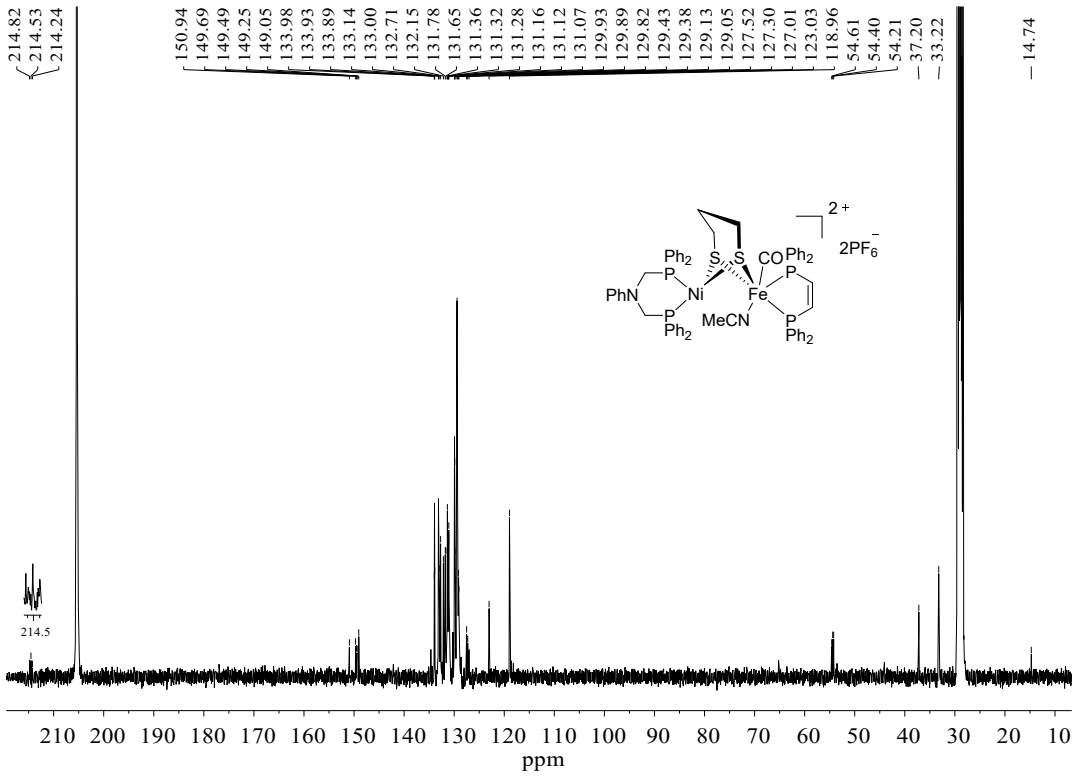

Fig. S40 ^{13}C NMR spectrum of [**9**](PF$_6$)$_2$

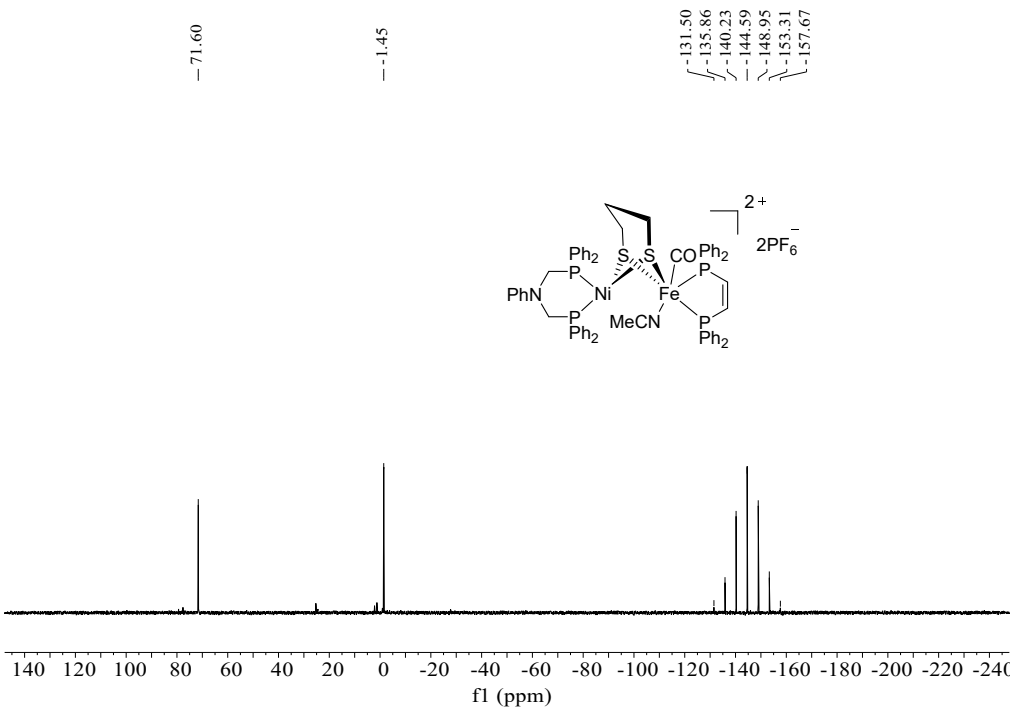

Fig. S41 ^{31}P NMR spectrum of [**9**](PF$_6$)$_2$

15. IR and ^{1}H (^{13}C, ^{31}P) NMR spectra of [**9**]$(BF_4)_2$

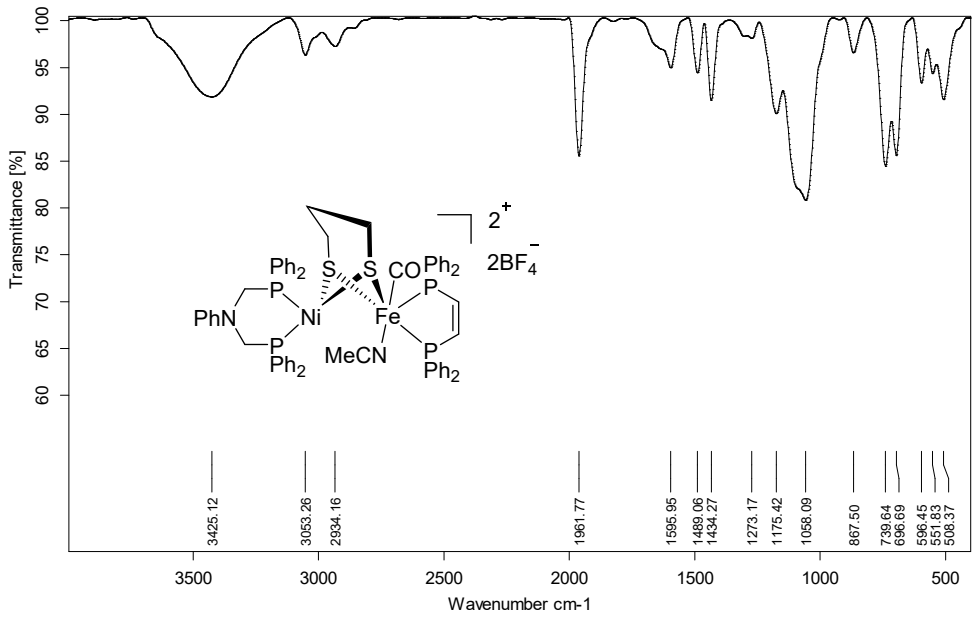

Fig. S42 IR spectrum of [**9**]$(BF_4)_2$

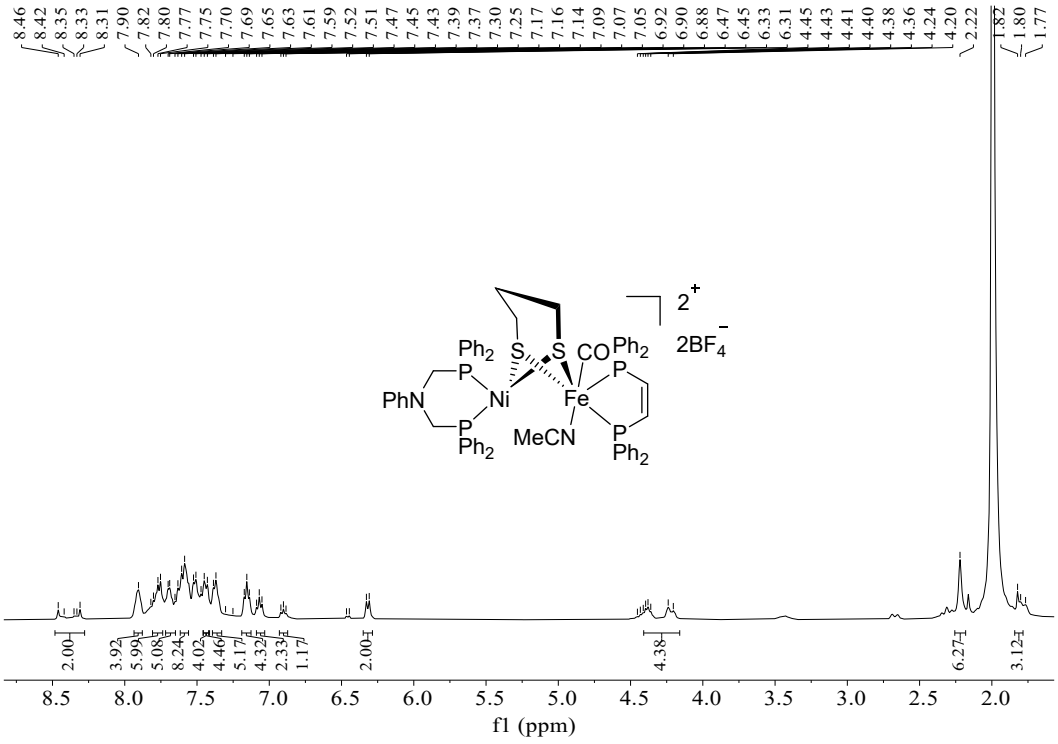

Fig. S43 ^{1}H NMR spectrum of [**9**]$(BF_4)_2$

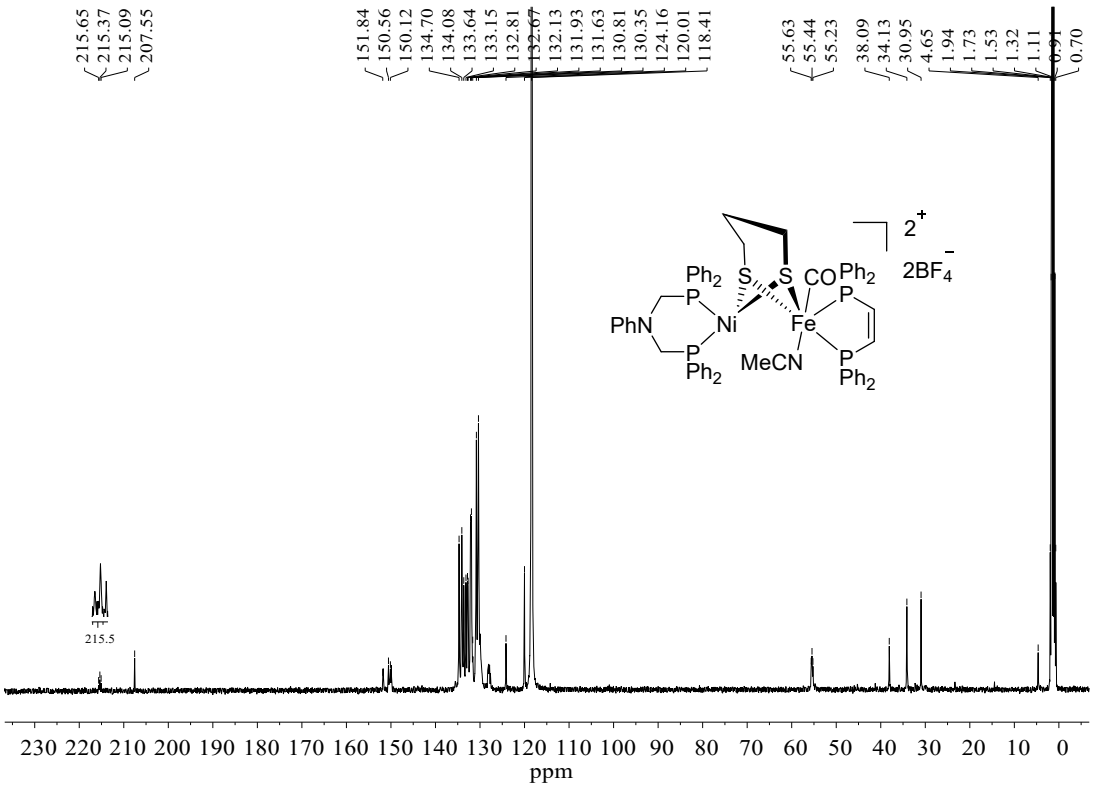

Fig. S44 ^{13}C NMR spectrum of [**9**](BF$_4$)$_2$

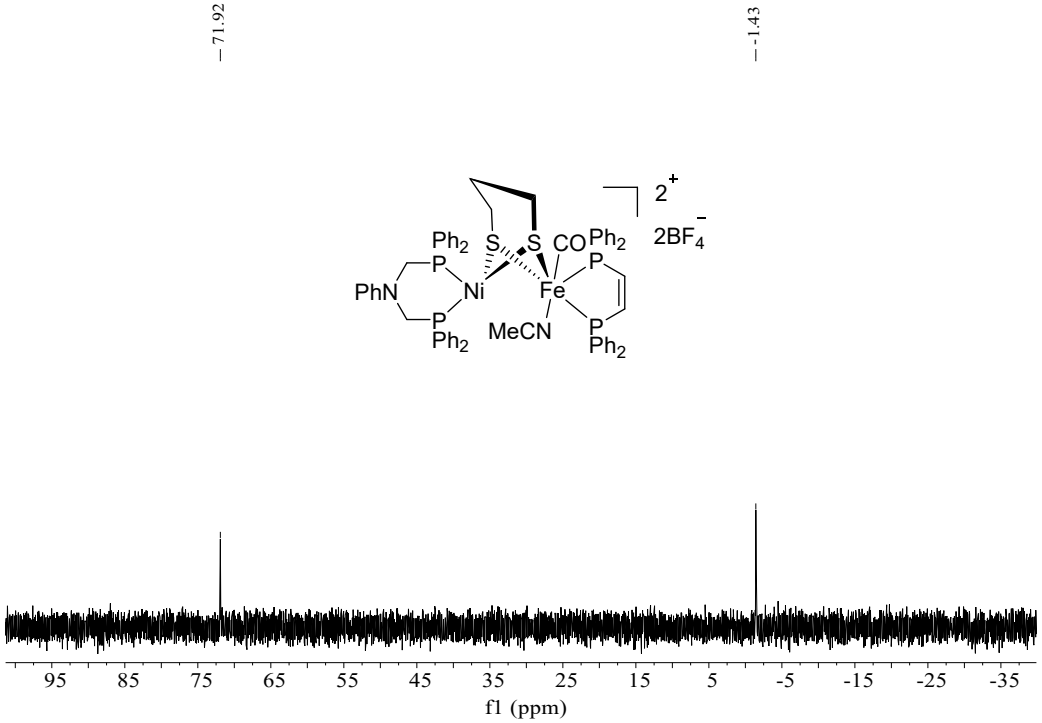

Fig. S45 ^{31}P NMR spectrum of [**9**](BF$_4$)$_2$

16. References

1 L.-C. Song, X.-F. Han, W. Chen, J.-P. Li and X.-Y. Wang, *Dalton Trans.*, 2017, **46**, 10003-10013.

2 L.-C. Song, Y.-X. Wang, X.-K. Xing, S.-D. Ding, L.-D. Zhang, X.-Y. Wang and H.-T. Zhang, *Chem. Eur. J.*, 2016, **22**, 16304-16314.